Hindawi
Mathematical Problems in Engineering
Volume 2024, Article ID 8374487, 15 pages
https://doi.org/10.1155/2024/8374487

Research Article

Development of a Digital Twin Framework for a PV System to Resolve Partial Shading

Bavithra Karunanidhi,[1] **Latha Ramasamy**,[2] **Albert Alexander Stonier**,[3] **and Charles Raja Sathiasamuel**[4]

[1]*Department of EEE, PSG Institute of Technology and Applied Research, Neelambur, Coimbatore 641062, Tamil Nadu, India*
[2]*Department of EEE, PSG College of Technology, Peelamedu, Coimbatore 641004, Tamil Nadu, India*
[3]*School of Electrical Engineering, Vellore Institute of Technology, Vellore-632014, Tamil Nadu, India*
[4]*Department of EEE, Thiagarajar College of Engineering, Thiruparankundram, Madurai 625015, Tamil Nadu, India*

Correspondence should be addressed to Bavithra Karunanidhi; bavithra@psgitech.ac.in

Received 9 July 2022; Revised 21 October 2022; Accepted 14 December 2023; Published 15 February 2024

Academic Editor: Zhiwen Chen

Digital twin (DT) is a prolific buzzword in this era, where digitization plays a significant role. The perception of solar energy harvesting has been gaining popularity with the advent of solar panels. Solar asset maintenance is a need of the hour for investors because of the smart city scheme and green building certificate evaluation for all industries, educational institutions, etc. Among the list of factors that reduce PV system efficiency, the issue of partial shading is a vital distress that must be resolved. This paper focuses on the development of a digital twin framework that is proactively driven by shading patterns and a proposed optimization-based reconfiguration embedded controller that electronically relocates the panel in the physical world. The real-time system has been created for a three-by-three series parallel panel arrangement. The proposed switching matrix controller achieves the maximum power, i.e., 40% of increased power output, row current difference is made almost zero from 3 to 4 A, and fill factor increases by 20% by reconfiguring the solar array. It is done based on a decision taken by a nature-inspired (equal irradiation distribution algorithm) or puzzle-based (skyscraper) optimization algorithm. Switching matrix controllers overcome the disadvantages of physical relocation. The users can query the digital twin build to know the historical performance and current operating conditions of the system. It can trigger alarms as early warnings and make predictions about possible system anomalies, if and when they occur using a digital twin.

1. Introduction

The widespread availability and affordability of solar energy position it as a plentiful and economically viable natural resource. Therefore, investigation has found a notable surge and endeavors focused on optimizing the harnessing of solar energy in recent times. Solar photovoltaic (PV) arrays stand out for their comparatively lower installation expenses when compared to other renewable energy sources. Currently, there is an increasing trend among people to adopt solar energy, driven by advancements in power semiconductor devices and government incentives aimed at promoting the use of renewable energy and creating a pollution-free environment. Digital twin (DT), a new technology after the Internet of things (IoT) and Industry 4.0, is a boon for asset maintenance and solves almost every reliability issue in a simpler way in every field. In agriculture [1, 2], it helps farmers to a greater extent by providing a better farm area understanding thus helping them in agricultural processes, i.e., irrigation, fertilization, pesticides, etc. This also helps them in making decisions and acting accordingly, and it reduces the manual task of observation. In the manufacturing sector [3–5], digital twins help in the designing and understanding of the end product checking the design and end product compatibility, thus giving space to reproduce originality and improve the performance. In other means, it creates carbon copy industry workers, machines, etc. related to real time, and hence, trial and error can be employed without any real-time production risk. In health care [6, 7], digital twins help to improve diagnostics and treatment for patients more economically in real time. The feasibility of medicine risk is simulated rather than tested in real time. In mobility

Table 1: Reliability issues in PV system.

Reliability issues	Overview
Partial shading [12]	Caused due to clouds (temporary), location of panels (permanent), tree, etc. It leads to hotspots, diode failure, cell degradation, reduced output, and at last pull-down panel life expectancy.
Dusting [13]	Soil deposition due to environmental conditions or seasonal changes, snow deposition or storm, etc. leads to output power loss, overvoltage, and deterioration of joints.
Hotspot [14]	Prolonged dust deposition, less maintenance, partial shading, and aging greatly reduce panel lifetime and create open circuit faults.
Diode fault [15]	Partial shading and overheating in a particular location led to reduced efficiency and damage to diodes.
Physical fault [16]	It includes installation damage, cell cracks, interconnection, issues, moisture penetration, yellowing ecosystem localities, etc. This can be fixed by maintenance.

[8, 9], one of the bottlenecks and delays in aircraft mobility is measured with a digital twin tool for tailored situations. The maintenance scenario for customers' waiting time, aircraft waiting for time, etc. is simulated and verified for worst cases. The future of mobility is autonomous cars, where the road model is made as the twin that helps in deciding a faster rate. Road system twin helps in the car manufacturing sector.

In energy, management [10, 11] is one of the key sectors where twin plays a major role in simulating energy demand and finding solutions to manage virtually in an efficient way. Net zero energy building can be implemented using this new technology of DT or digital shadow. Yet another role of the twin in the energy sector is renewable energy-related computational DT framework to find a way to optimize the flow of power.

Creating a digital twin for the PV system enables the stakeholders to better assurance of the payback period. This is achieved by proactive monitoring and scheduled maintenance. During operation, it addresses the reliability issue without human intervention. MATLAB driven by real-time parameters and analyzed information for shading is used to realize the digital shadow for the PV system. PV array is dependent on various intermittent reliability problems like shading, dust, bird, drop, contamination, and snow as given in Table 1.

The PSC (partial shading condition) disturbs the characteristics curves of the PV array. It is one of the important issues if addressed, can improve output power to a greater extent, and improves the life expectancy of panels, thus ensuring a promised payback period [17, 18]. Since the output generated by a single PV is relatively lesser, multiple panels must be used. So, to increase the power output, the panels are interconnected in several ways.

Many kinds of panel arrangements have been adopted in various kinds of literature. In series–parallel (SP) [19], interconnections are less, economical, easy to build, and occupy less space and is a traditional method that is widely followed. Total cross tied (TCT) [20] is connected in such a way that voltage across the cell of PV remains the same. In honey comb (HC) [21], these algorithms were introduced to achieve optimal power generation from solar panels. They facilitate the configuration of arrays in a manner that ensures the attainment of maximum power by evenly distributing shadows among the panels, thereby minimizing variations in row currents ensuring simplicity in arrangement of panels and its also ease the analysis of the reconfiguration technique.

Due to partial shading conditions, the row currents of each panel can vary, and this will lead to hot spots in the panels. It might reduce the total lifetime of the PV Panel. To increase the lifetime, bypass diodes can be used. These diodes during partial shading conditions bypass the panel and allow the current to flow through the diode. This technique might increase the lifetime of the panel, but it induces a reduction in the total power yield. Since diodes are used to bypass the panels, this decreases the total output voltage and causes heat losses thus reducing power production. This is because the partial power produced by the panels is not utilized since they are bypassed.

To improve power production, two types of configurations were proposed, namely, static configuration [22] and dynamic configuration. In static configuration, the physical position of the solar PV panel is altered one time based on the resultant obtained pattern, whereas in dynamic configuration [23], the electrical connections of the panels are rewired using a switching matrix controller [16, 24].

Static reconfiguration involves many kinds of panel array arrangement as discussed above. Apart from the panel arrangement pattern, a different mathematical puzzle to attain a pattern is discussed. Skyscraper [25] is based on row, height, and column for the building. This provides better dispersion of shading patterns for all kinds of arrangements of panels and takes less time for evaluation. Sudoku [26, 27] is a logic number-based puzzle, every column and row matrix digits are accommodated and the objective function is achieved, but it seems to be difficult for the increased size of the matrix. Dominance square [28] is based on number placements that position an alphabet. This reconfiguration method seems to have less mismatch loss, and the fill factor is high.

In contradiction, dynamic array reconfiguration has been adopted for electronic switching to reconfigure the array. The pattern of switching is decided by various metaheuristic algorithms. The particle swarm optimization (PSO) [29, 30] is inspired by swarms moving toward food, and it is the most widely used algorithm, but the time consumption and panel shading pattern adaptation are less. In genetic algorithms [31], the fitness function and parameter choosing play a crucial role in accomplishing better optimization convergence. The bypassing of the panel with the aid of shading chances is

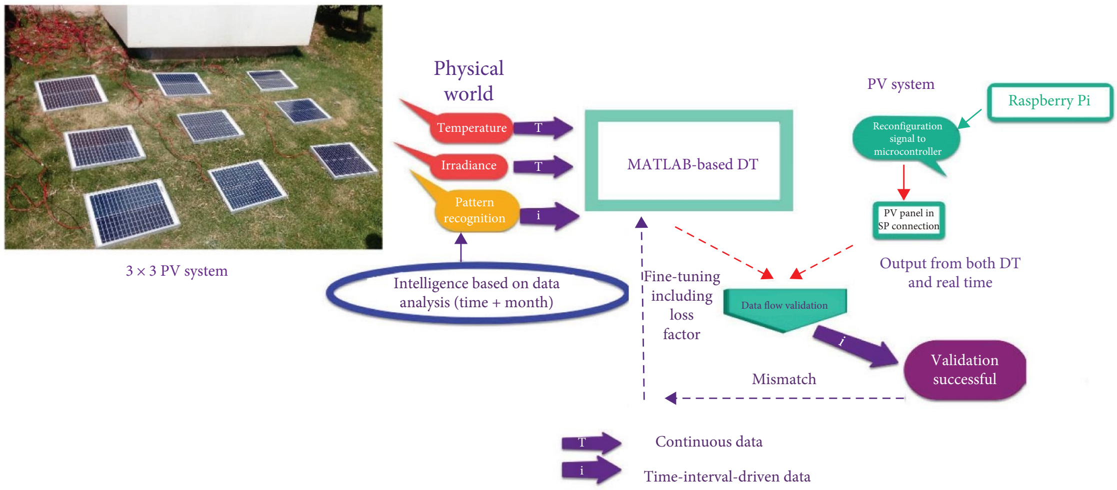

Figure 1: Proposed digital twin framework with physical world.

reduced by this approach of optimization. Hence, the output power is enhanced, but it involves more understanding. In addition to this, grey wolf [32], grasshopper, butterfly, ant colony, and bee colony algorithms are also dealt with in various literature. These algorithms were proposed to obtain the highest potential from the solar panels and help to configure the arrays by dispersing the shadow equally among the panels to reduce the variation in row currents [33]. Among these algorithms, in this paper, PSO-inspired equal irradiance distribution (EID) algorithm is developed and employed to reconfigure panels electronically. The skyscraper algorithm is also used to compare the performance with EID.

From the literature review, it is evident that electronic reconfiguration of panels in real-time hardware using the proposed optimization-based switching matrix controller is not highlighted. So far, the advent of a digital twin for asset maintenance and addressing partial shading in PV systems has not been emphasized. This paper presents the development of a digital twin framework using MATLAB, serving as both a data-driven model and the basis for an embedded switching matrix controller in a real-time physical system. The implementation of this framework enhances the output of PV panels experiencing partial shading. The performance of the controller was evaluated across six distinct shading scenarios. In this paper, Section 3 presents the digital twin framework, Section 4 elucidates the physical real world, Section 5 discusses the salient results obtained, and Section 6 concludes the work along with the future scope.

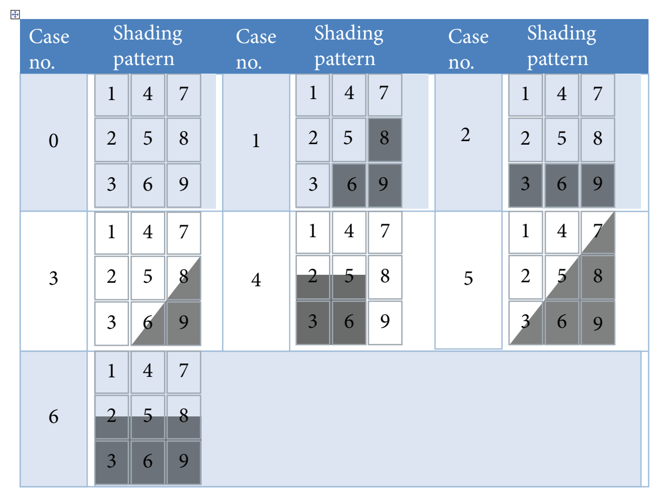

Figure 2: Shading pattern.

Table 2: Attributes of PV panel.

Parameter	Rating
P_{max}	20 W
V_{oc}	22.5 V
V_{mpp}	19.25 V
I_{sc}	1.11 A
I_{mpp}	1.04 A

2. System Description—Development of Digital Twin Framework

The DT framework is developed using MATLAB simulation. The overview of the DT framework is shown in Figure 1. Environmental conditions like real-time irradiation and ambient temperature [24] of the panel locality are given as continuous input for an hour to simulate a digital panel. Shading pattern information is obtained based on the probability of occurrence of shade in the location (11°03′55.0″N, 77°05′35.9″E). The pattern of shade data is given as time interval input based on historical seasonal and day sun rotation. The shading probability is formulated using a simple camera, and the study is carried out the for last year (all seasons). The shading pattern taken for further analysis is shown in Figure 2 with Case 1 as No Shading (NS), Case 2 as Right Ladder (RL), Case 3 as Bottom Row (BR), Case 4 as Right Triangle (RT), Case 5 as Left Square (LS), Case 6 as Right Half Triangle (RHT), and Case 7 as Lower Half Bottom (LHB).

The attributes of the outdoor experimental PV system are matched with the simulated panel as shown in Table 2.

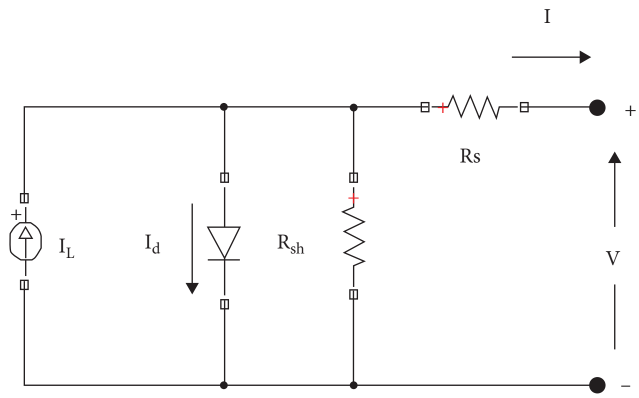

FIGURE 3: Five-parameter model of panel.

The digital panel takes all its input from a real-time environment, takes decisions based on algorithm output, reconfigures the panel, and ensures improved performance in the digital world. In the physical world, the reconfiguration signal is sent by Raspberry Pi which runs an algorithm based on the pattern of shade occurrence and produces power. The digital twin and real-world output mismatch due to environmental factors and losses is incorporated as a loss factor by fine-tuning during an initial trial run, and the similar performance of the physical world the and digital asset is guaranteed.

2.1. Modeling of Panel and Simulation of 3 × 3 Solar Panel in Series Parallel Connection. A multivariable model using photons emitting source (I_L), semiconductor rectifying device, sequential resistance (R_{se}), and bypass resistance (R_{bypass}) to represent I–V characteristics of the modules is employed in this work is portrayed in Figure 3. The semiconductor rectifying device current and voltage characteristics for a module are demarcated by Equations (1) and (2).

$$I_d = I_0[\exp(V_d/V_d) - 1], \tag{1}$$

where I_d = Electron flow (A), V_d = potential (V), and I_0 = breakdown current (A)

$$V_T = KT/q \times \mathrm{nI} \times N_{cell}, \tag{2}$$

where nI = fitting factor, a number close to 1.0; K = Boltzman's constant = 1.3806e^{-23} J/K; q = Electron charge = 1.6022e^{-19} C; T = Cell temperature (K); and N_{cell} = Number of cells connected in series in a module.

Here, the simulation is done on a 3 × 3 solar array without the presence of the diodes, and then, it is compared with the same array with the presence of diodes. The irradiation and temperature input data from the pyranometer are fetched by MATLAB, and then, this is linked to the irradiation of the solar panel in the Simulink block. The simulation block is shown in Figure 4.

During the simulation, the solar array voltage, individual row current, and solar array currents were measured and stored for later analysis. To obtain the P–V and I–V curves, the solar array is connected to voltage voltage-regulated source, and a ramp signal is given. The ramp has a slope of three, and this causes the voltage source to provide a range of voltage starting from zero.

2.2. Design of Data-Driven Twin. Pyranometer fed the direct irradiation, diffused irradiation, and temperature data to the data logger [34] where data is logged concerning GPS timing. The simulation is designed to be executed using the temperature and irradiation data from the real world. It is driven by shading pattern data fetched from seasonal and day sun rotation details mapping with current GPS timing making intelligence concerning the real world. MATLAB simulation-based data-driven twin is used for running simulations not only for test conditions but also for real-time conditions. It can further able to simulate anticipated conditions that may occur in the future. Thus, the twin acts as a software virtual asset to a real PV system. It works by incorporating the physical world and creates a digital shadow as exposed in Figure 5.

3. Experimental Setup—Real-Time Hardware

For experimental verification, the nine solar panels were arranged in a series–parallel topology as revealed in Figure 6. Each junction in the panel was integrated into a solar array reconfiguration panel. The signals to trigger the particular relay depending on the shading pattern were fed from the solar array control panel. The relay triggering signal is enabled by the control signal from Raspberry Pi, which runs an algorithm that decides the reconfiguration position of PV panels. The solar array control panel has 5 V regulators, whereas the solar array relay panel does not have a regulator. So the voltage source for the relays was taken from a regulated power supply (RPS).

The shading effect for cases is realized in Figure 7 (for experimental purposes, the shades are created purposefully inspired by real-time shading patterns concluded from data analysis).

3.1. Switching Matrix Controller. The switching matrix controller consists of a switching matrix board controlled by an ATmega16 microcontroller. Matrix switching circuit is inspired by the architecture of a field programmable gate array (FPGA).

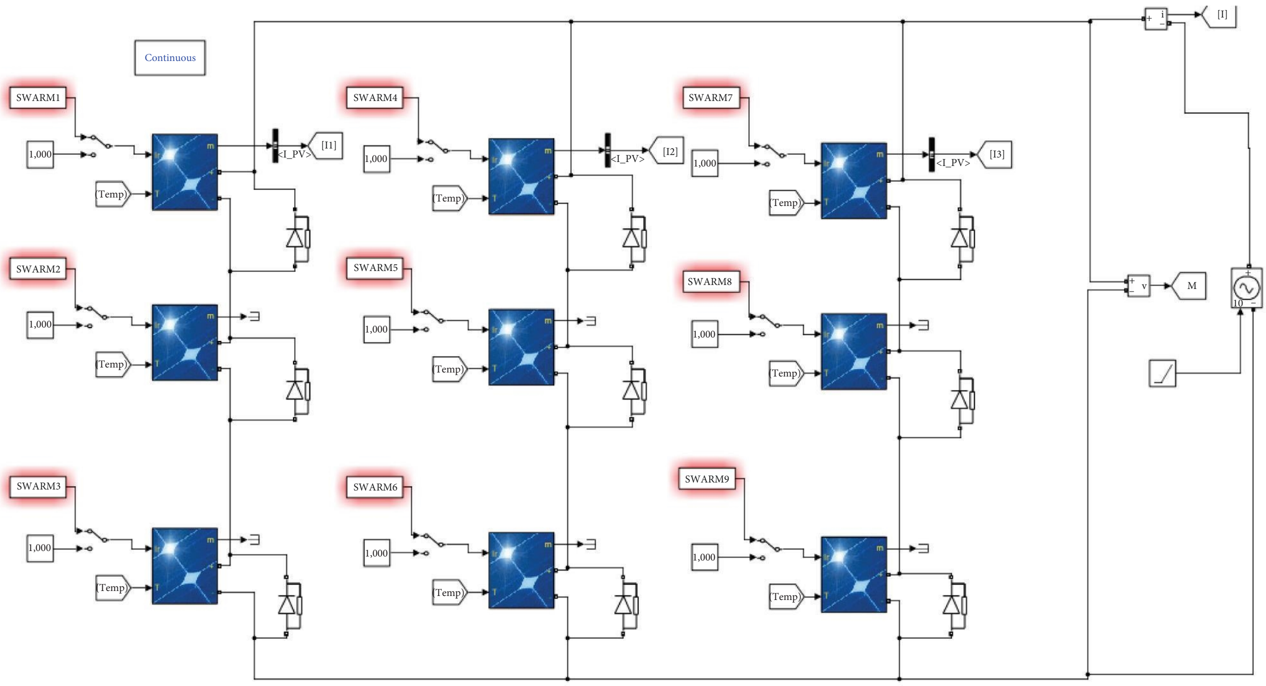

FIGURE 4: MATLAB simulink diagram.

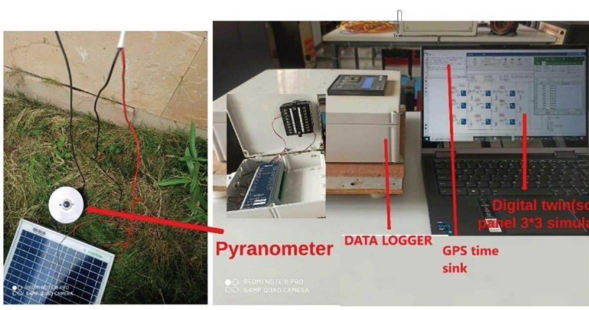

FIGURE 5: DT setup.

FIGURE 7: Case 3 and Case 6 solar panel shading arrangement.

FIGURE 6: 3×3 solar panel arrangement.

When comparing the hardware model and the FPGA, the programmable interconnect in the FPGA would be the switches, the logic block would be the solar panels, and the wires running in between the logic blocks would be the bus bars as shown in Figure 8.

The relay operating status of six different real-time shading pattern cases taken for consideration, it is noted that in any condition only 2 CB are ON in the channels from A to F sequence. Also, 3 CBs are ON continuously in the high and low channels. Under normal conditions, channel A is used to connect the low terminal of the first panel to the high terminal of the second panel. Channel B is used to connect the low terminal of the second panel to the high terminal of the third panel. Channel C is used to connect the low terminal of the fourth panel to the high terminal of the fifth panel. Channel D is used to connect the low terminal of the fifth panel to the high terminal of the sixth panel. Channel E is used to connect the low terminal of the seventh panel to the high terminal of the eighth panel. Channel F is used to connect the low terminal of the eighth panel to the high terminal of the ninth panel. The high terminal channel connects the high terminals of the first, fourth, and seventh solar panels. The low channel connects the low terminal of the third, sixth, and ninth solar panels. The relay status for Cases 3 and 5 is shown in Figure 9.

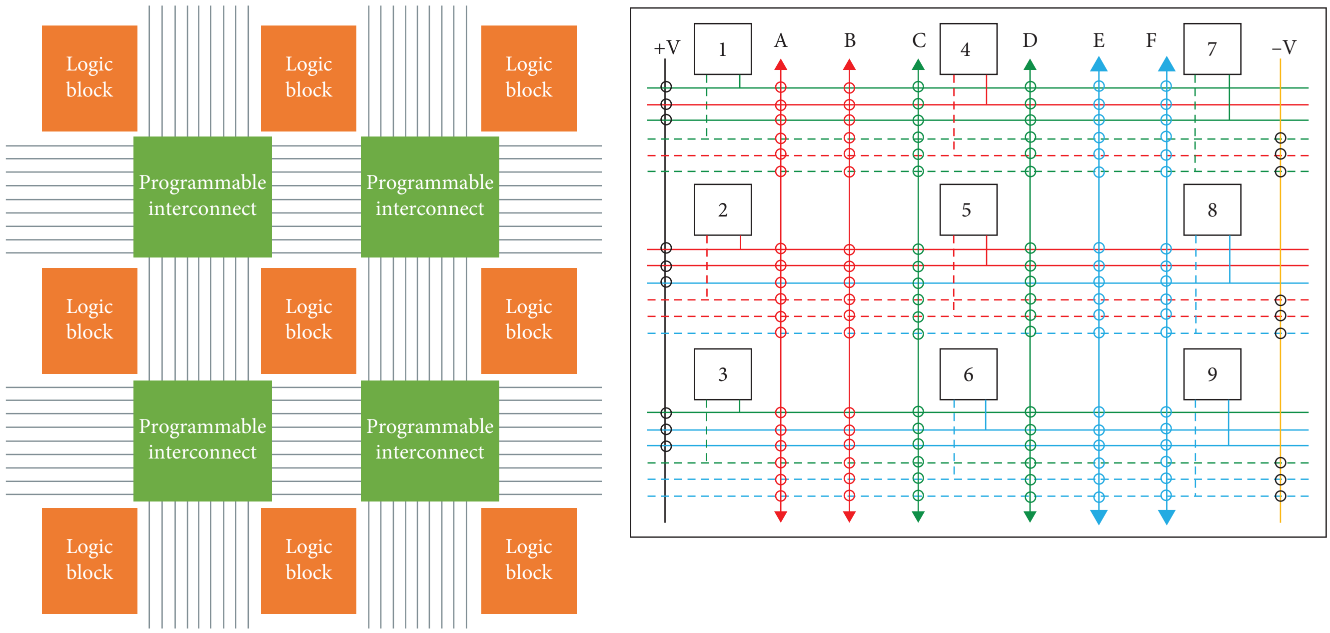

Figure 8: FPGA-inspired switching matrix arrangement.

Positive	A	B	C	D	E	F	Negative	Positive	A	B	C	D	E	F	Negative
0	0	0	1	0	0	0		0	0	0	1	0	0	0	
0	0	0	0	0	1	0		1	0	0	0	0	0	0	
0	0	0	0	0	0	1		0	0	0	0	0	0	1	
	0	0	0	1	0	0	0		0	0	0	1	0	0	0
	0	0	0	0	0	1	0		0	0	1	0	0	0	0
	0	0	0	0	0	0	1		0	0	0	0	0	0	1
1	0	0	0	0	0	0		0	0	0	0	1	0	0	
1	0	0	0	0	0	0		1	0	0	0	0	0	0	
0	0	1	0	0	0	0		1	0	0	0	0	0	0	
	0	0	1	0	0	0	0		0	0	0	0	0	0	1
	0	0	0	0	1	0	0		0	0	0	0	1	0	0
	0	0	0	0	0	0	1		1	0	0	0	0	0	0
0	0	0	0	1	0	0		0	0	0	0	0	1	0	
1	0	0	0	0	0	0		0	0	1	0	0	0	0	
0	1	0	0	0	0	0		0	1	0	0	0	0	0	
	0	0	0	0	0	0	1		0	0	0	0	0	1	0
	1	0	0	0	0	0	0		0	0	0	0	0	0	1
	0	1	0	0	0	0	0		0	1	0	0	0	0	0

Figure 9: Electronic switches status diagram for Cases 3 and 5.

The requirement of switches is decided using Equation (3)

$$\text{No.} = (2 \times x \times y) \times (((x - 1) \times y) + 1), \tag{3}$$

where No. is the quantity of electronic switches required, x is the count of rows, and y is the count of columns of the solar array. Thus, the overall hardware setup is shown in Figure 10.

3.2. Reconfiguration Algorithm. Most prevailing man-made one-time relocation and switching relocation methods have been formulated based on numerical riddles that are not accordant with both symmetrical and unsymmetrical PV arrays. A new switches-based repositioning option is PSO-based EID and a skyscraper puzzle for arrays repositioning are developed in this paper. It is simulated, implemented, and tested.

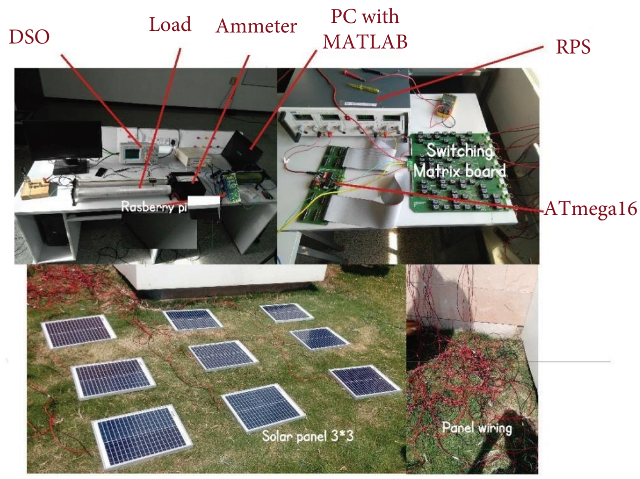

Figure 10: Overall hardware arrangement.

3.2.1. Equal Irradiance Distribution (EID) Algorithm. The algorithm is inspired by PSO [22]. The objective function is given in Equation (4), which is intended to obtain maximum power with a row current difference mitigation, less power loss, and increased fill factor.

$$\text{Objective Function}, F = \sum_{1}^{m} I_{RD}, \tag{4}$$

where m is several rows.

PSO finds optimal shade dispersion for a matrix of the panel with the objective function to attain minimum row current difference with maximum power that in turn reduces power loss and increases fill factor. Constraints for the optimization problem taken into consideration are minimum switching and equal shade dispersion. PSO-based EID is versatile and sturdy with lesser analytical time because of parallel computation. Even though it randomizes the position vector using the randi function at the beginning, in the manner of velocity update this method converges and provides a better shade dispersion pattern.

The algorithm for the EID is as follows:

Step 1: Instigation phase: PV array size with $x \times y$ is initialized. The cognitive constant C1, C2, and inertia weight W are computed as time-varying using Equations (5–7).

The upper and lower limits are $0.2 < \text{C1}, \text{C2} < 2$, and $0.2 < \text{W} < 1$.

$$W = W_{\max} - ((W_{\max} - W_{\min}) \times (1 - \text{Current iteration}/\text{Max iteration})), \tag{5}$$

$$\text{C1} = C_{\max} + ((C_{\min} - C_{\max}) \times (\text{Current iteration}/\text{Maximum iteration})), \tag{6}$$

$$\text{C2} = C_{\min} + ((C_{\max} - C_{\min}) \times (\text{Current iteration}/\text{Maximum iteration})). \tag{7}$$

Step 2: Collective matrix generation for swarms: Initialize the swarm matrix with particles, and the starting velocity for swarms is computed using Equation (8).

$$\text{Velocity}(\text{i}) = 1 + \text{round}\,(\text{rand}, 9), \tag{8}$$

Step 3: Feeding irradiance data: The data are fed using a pyranometer arrangement and present row current difference that evaluates the objective function.

Step 4: Position matrix evaluation: The particle position is evaluated in the matrix by following step 3 using the data of irradiance pattern and row current difference. The fitness function evaluation is done using the ismembertol MATLAB function to evaluate the difference of row currents with some tolerance for position vectors at the time function calling.

Step 5: Velocity update: The velocity is rationalized using Equation (9).

$$Vk + 1 = W \times Vki + [\text{C1} \times \text{rand1} \times (\text{Pbest} - \text{Ski})] + [\text{C2} \times \text{rand2} \times (\text{Gbest} - \text{Ski})], \tag{9}$$

where $Sk + 1 = \text{Ski} + Vk + 1$. The first part of the Equation (9) is known as the cognitive that represents earlier velocity which provides the needed momentum for particles to move across the search space. The second part is the social part which represents the previous personal thinking of each particle. The cognitive part encourages the particle to move toward its own best position so far.

Step 6: Objective function evaluation: The obtained position vector is evaluated to meet the objective function and constraints, i.e., shade is dispersed equally with minimum switching.

$$\text{Fitness Function } F = \sum_{1}^{m} I_i - I_j, \tag{10}$$

where m = number rows of panel in PV system = 1, 2,…, i, j, …, m (i, j = consecutive rows in PV system).

Step 7: Check for ending: If the objective function is met, then the algorithm terminates, or steps 5 and 6 are repeated. For simulation purposes, the algorithm can run in MATLAB, but, for outdoor experimental verification, this algorithm is taken care of by Raspberry Pi 3, a minicomputer. The algorithmic flowchart is illustrated in Figure 11.

3.2.2. Skyscraper Algorithm. The skyscraper game [16] is fundamental for the algorithm for repositioning panels. Skyscraper is a puzzle that places edifices along the sides with the help of some hints based on X × X grids. Skyscrapers are to be positioned within a grid such that each square accommodates a skyscraper with a height ranging from 1 to X. The challenge is to arrange them in a way that ensures no two skyscrapers in the same row or column share the same number of floors. The visible quantity of edifices, as viewed from

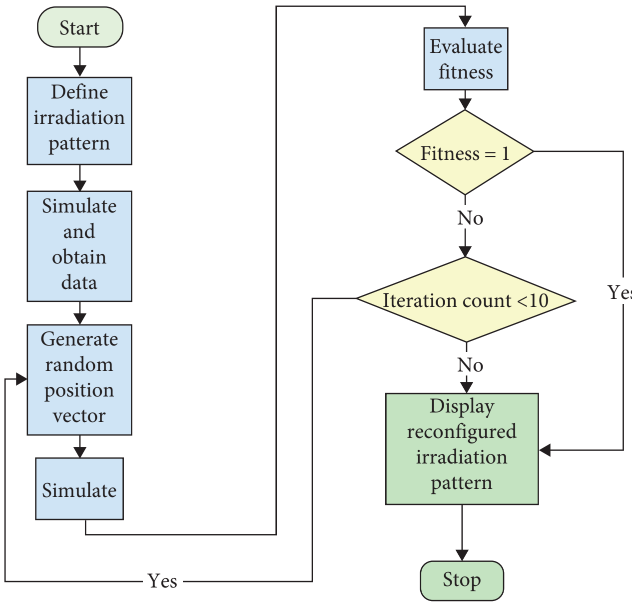

Figure 11: EID algorithm flow diagram.

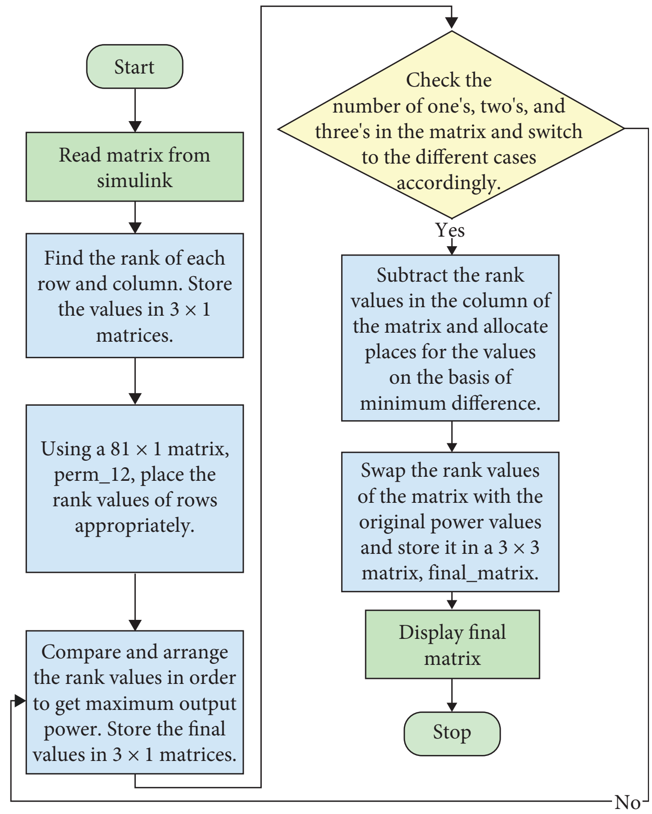

Figure 12: Skyscraper algorithm flow diagram.

the direction of each hint, is equal to the value of the hints. The higher edifices block the view of the lower edifices located behind them. In this paper, a 3×3 skyscraper puzzle with three columns and three rows is considered. One-floor to three-floor skyscrapers are placed in each row and column accordingly. The flow diagram for the skyscraper algorithm is represented in Figure 12.

4. Results and Description

The maximum power that has been extracted at different irradiation levels is inferred from the I–V and P–V curves.

4.1. Digital Twin—Software Results

4.1.1. Before Reconfiguration. The simulation results have been taken for all seven cases, and Case 6—Right Half Triangle (RHT) has been discussed in detail. The peak power generation for the array in Case 6 without the presence of a diode is 101.4 W and in the presence of a diode is 104.1 W is recorded in Figure 13.

There is a slight difference in power delivered by the solar panel in the presence of a diode; however, two local peaks and one global peak are present in the P–V curve. The peak power tracking controller will fail to detect the global peak and will operate at the first local peak whose output power is closer to 60 W. Thus, about 44 W of power is not utilized. Output power can be enhanced to nearly 42%. Hence, it is imperative to reconfigure the solar array to extract the highest output power.

4.1.2. Twin Response after Reconfiguration. The power difference at the initial peak in the P–V curve and the maximum difference of the P–V curve before and after reconfiguration are tabulated in Table 3. In Figure 14, the blue curve represents curves before reconfiguration while the red curve represents curves after the reconfiguration of the solar array.

Case 1: (Right Ladder) In Figures 14(a) and 14(b), it is observed that, before reconfiguration, there are many crests in the power curve, and a typical maximum power point tracker will detect the initial crest as the global one and will operate at that point thus providing only 58 W. After reconfiguration, only one global point is present in the power curve. So the tracker will now provide an output power of 131 W. The output power has increased by 73 W, i.e., 56% output enhancement is possible for this case after reconfiguration.

Case 2: (Bottom Row) Figures 14(c) and 14(d) depict the I–V and P–V curves. The initial maximum power before reconfiguration is 117 W, and it is noteworthy that it has two crests, in contrast to the three crests observed in the right ladder pattern of shading. Following reconfiguration, the maximum extractable power increases to 131 W.

Case 3: (Right Triangle) In Case 3, illustrated in Figures 14(e) and 14(f), the power curve displays three peaks before, and this reduces to two peaks after reconfiguration. 58 W is obtained at the initial crest in Case 3 in the initial position, whereas after reconfiguration, 132 W of power is obtained. Despite the existence of numerous crests in the P–V curve, the tracker functions at the initial crest, as explained earlier. Consequently, 104 W of power is obtained, representing a rise of 46 W of power.

Case 4: (Left Square) Figures 14(g) and 14(h) illustrate curves of Case 4. Notably, the number of peaks remains consistent in both cases. The maximum power stands at 56 W before and increases to 103 W after reconfiguration.

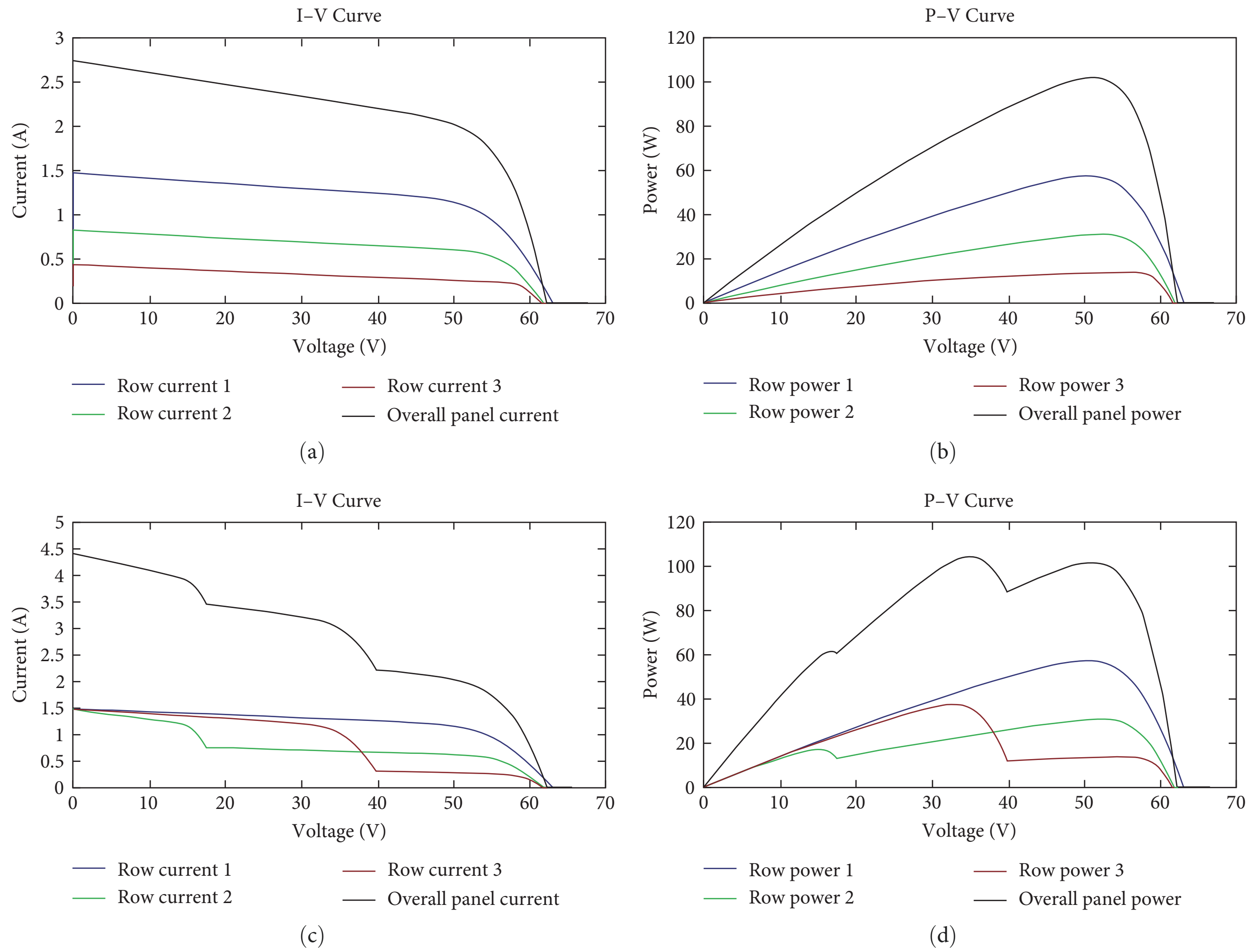

Figure 13: I–V and P–V curves of Case 5 (left square). (i) Without diode (a, b), (ii) with diode (c, d) in SP connection.

However, a comparison of both curves reveals that the power at the initial crest is 56 W, whereas the power is 9 W after repositioning of panels based on algorithm results. Consequently, connecting repositioned panels to the tracker results in an output power of 7 W less than that before reconfiguration. This discrepancy is attributed to the algorithm fitness function evaluation and randomization limitations inherent to this shading pattern.

Case 5: (Right Half Triangle) Figures 14(i) and 14(j) illustrate the curves for Case 5. The numerous peaks in the power curve before reconfiguration are consolidated into a single global peak after the reconfiguration, resulting in an increased output power of 54 W.

Case 6: (Lower Half Bottom) Figures 14(k) and 14(l) display the I–V and P–V curves for Case 6. The power experiences a boost of 45 W; along with that, numerous crests are consolidated into one global crest. Regarding the cases discussed above, the output power sees an increase ranging from ~40 to 50 W, representing an enhancement of nearly 30%–45%.

4.1.3. Performance Comparison of Algorithms. Both the EID and skyscraper algorithms give almost similar reconfiguration for the above six cases, and hence, power gain comparing both algorithms is of the same watts as mentioned in Table 3. Still, the decision-making time for both algorithms is compared. It proves that the skyscraper algorithm provides a fast response but requires high mathematical computation knowledge. It is very difficult if the matrix size is increased compared to PSO based EID algorithm.

The results show that the EID delivers improved shade scattering across the full array, thus resulting in minimized discrepancies like mismatch losses to enhance efficiency power and is easy to compute. Hence, for network reposition controller implementation, EID-based PSO is adopted, and experimental verification is carried out.

In general, skyscraper is a static type of array reconfiguration; it also involves the physical relocation of panels, but the pattern of shading is versatile; hence, the dynamic type EID algorithm for array reconfiguration by altering the electrical

Table 3: Irradiation pattern before and after reconfiguration with position vector and power difference.

Case no.	Initial panel position	Number of peaks	Irradiation pattern (W/m^2)	Position after reconfiguration	No. of peaks after reconfiguration	Power difference at first peak (W)	Power difference at global peak (W)
1	1 4 7	3	1000 1000 1000	5 3 9	1	+73 W	+42 W
	2 5 8	—	1000 1000 0200	2 7 8	—	—	—
	3 6 9	—	1000 0200 0200	4 1 6	—	—	—
2	1 4 7	2	1000 1000 1000	2 9 5	1	+14 W	+14 W
	2 5 8	—	1000 1000 0500	4 3 7	—	—	—
	3 6 9	—	1000 0200 0500	8 6 1	—	—	—
3	1 4 7	3	1000 1000 1000	6 2 5	2	+46 W	+30 W
	2 5 8	—	1000 1000 0500	9 1 4	—	—	—
	3 6 9	—	1000 0500 0200	8 3 7	—	—	—
	—	—	—	—	3	—	—
4	1 4 7	3	1000 1000 1000	9 4 5	—	−7 W	+18 W
	2 5 8	—	0500 0500 1000	8 7 3	—	—	—
	3 6 9	—	0200 0200 1000	1 2 6	—	—	—
5	1 4 7	3	1000 1000 0500	8 4 5	1	+54 W	+32 W
	2 5 8	—	1000 0500 0200	9 1 3	—	—	—
	3 6 9	—	0500 0200 0200	4 2 7	—	—	—
6	1 4 7	3	1000 1000 1000	8 6 1	1	+45 W	+38 W
	2 5 8	—	0500 0500 0500	5 9 4	—	—	—
	3 6 9	—	0200 0200 0200	2 3 7	—	—	—

connection of switches proves to be a better option compared to one-time skyscraper-based array reconfiguration.

4.2. Physical World Output—Hardware. To obtain characteristics curves, the potential between the solar panel arrangement and the flow of electrons through the shunt resistor were measured using the two channels of a digital signal oscilloscope (DSO). Using a rheostat, the load was decreased from maximum value to minimum value to obtain curves. As the resistance is decreased to the minimum, the solar array is said to be in short circuit condition. When the resistance is increased to the maximum values, then the solar array is in open circuit condition. Thus, when resistance decreases, the current increases and the voltage decreases, and vice versa. The waveform from the DSO is obtained by storing the data in a USB and plotted using MATLAB. The reconfiguration model is shown in Figure 15.

Note that, in all the cases discussed above, if the circle is colored inside, then that particular relay is ON. By compiling the status of the relays in every case, it is observed that not all relays are utilized for switching. Based on the complexity of the cases of irradiation pattern, the number of relays that is not utilized can be reduced in number. The hardware model is designed to accommodate 126 switches; however, only 74 are used in the practical model to verify the results that were obtained for the different cases of irradiation pattern. After obtaining the graphs for each case from the DSO, the data are fed to MATLAB for processing. The V and I waveforms are smoothed using the moving average known as the moving mean method. The power is computed by taking voltage time current at each time step. The voltage, current, and power values are recorded, and the graphs are plotted. Power is plotted against voltage to obtain the P–V curve, while current is plotted against the voltage to obtain the current–voltage curve.

In every Case 2–7, there is a substantial yield surge, particularly in Cases 4 and 6 given in detail in Figure 16.

Case 3: (Right Triangle - RT) Resultant graph shows that, before reconfiguration (Figures 16(a) and 16(c)) the output of the panel in the first peak is nearly 47 W, but after reconfiguration (Figures 16(b) and 16(d)), power at the global peak is nearly 93 W, i.e., after switching matrix controller involvement, nearly 46 W of output is increased.

Case 5: (Right Half Triangle - RHT) Resultant graph shows that, before reconfiguration (Figures 16(e) and 16(g)), the output of the panel in the first peak is nearly 30 W, but after reconfiguration (Figures 16(f) and 16(h)), power at the global peak is nearly 47 W, i.e., after switching matrix controller involvement, nearly 17 W of output is increased.

The position vector before and after reconfiguration with power difference is tabulated in Table 4.

Table 4 demonstrates the power modification amid the no-shading case and six different cases (real-time shading cases taken for analysis) before and after reconfiguration at the first local peak and the global peak. From the graphs, the local peaks that appear in the P–V graphs before reconfiguration have either disappeared in the P–V graphs after reconfiguration or at least

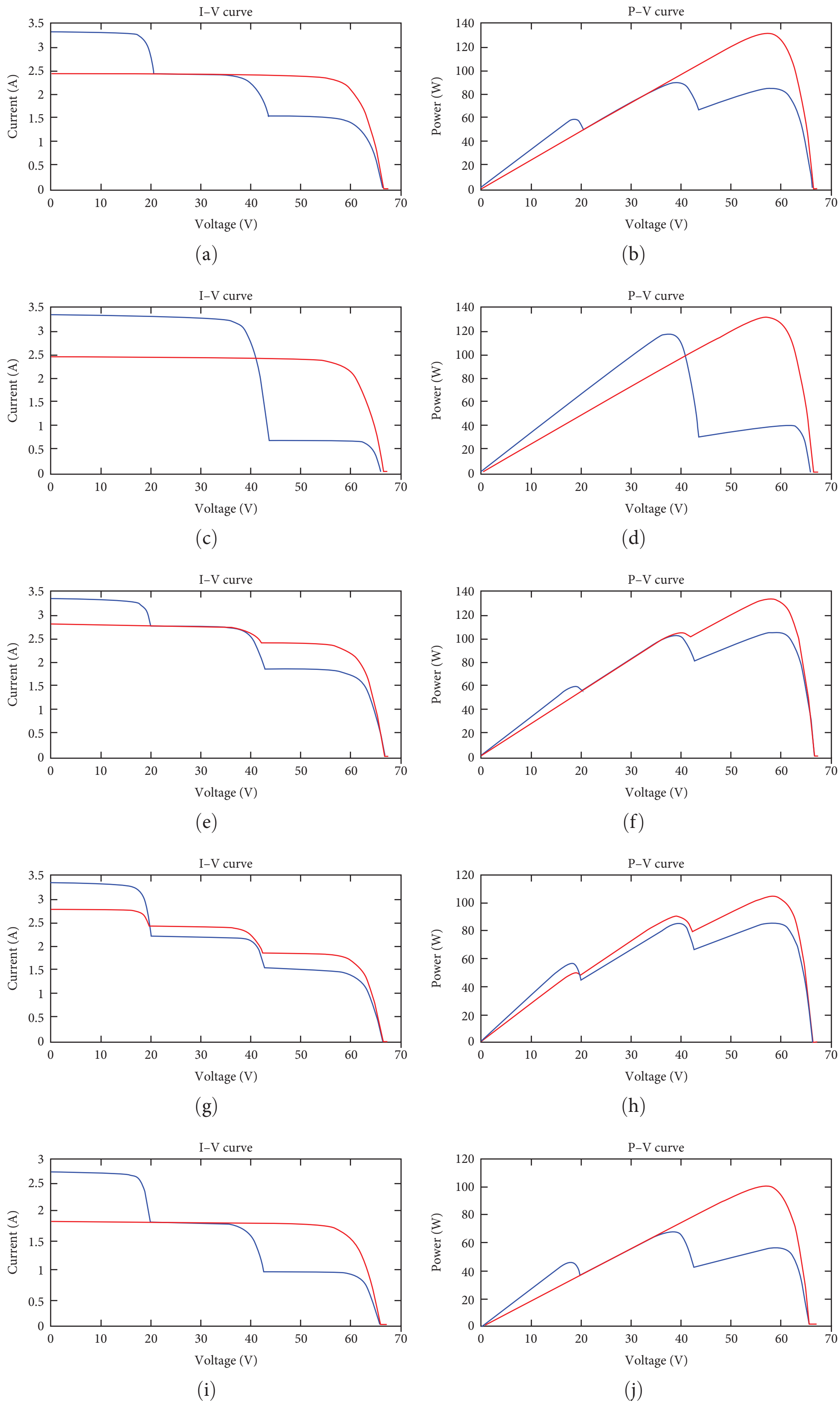

Figure 14: Continued.

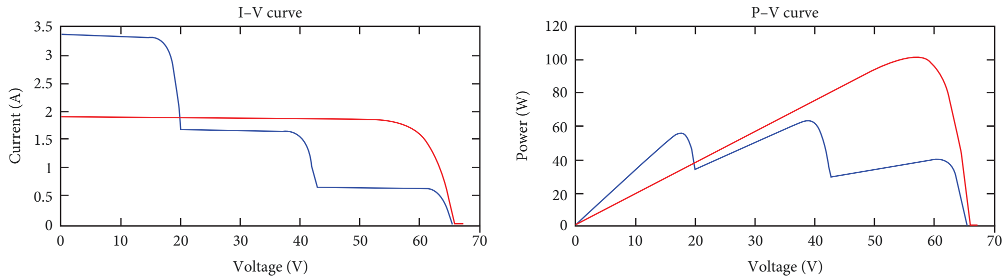

(k)

(l)

Figure 14: I–V and P–V curves (i) before (blue) reconfiguration, (ii) after (red) reconfiguration for Cases 1–6 (a–l).

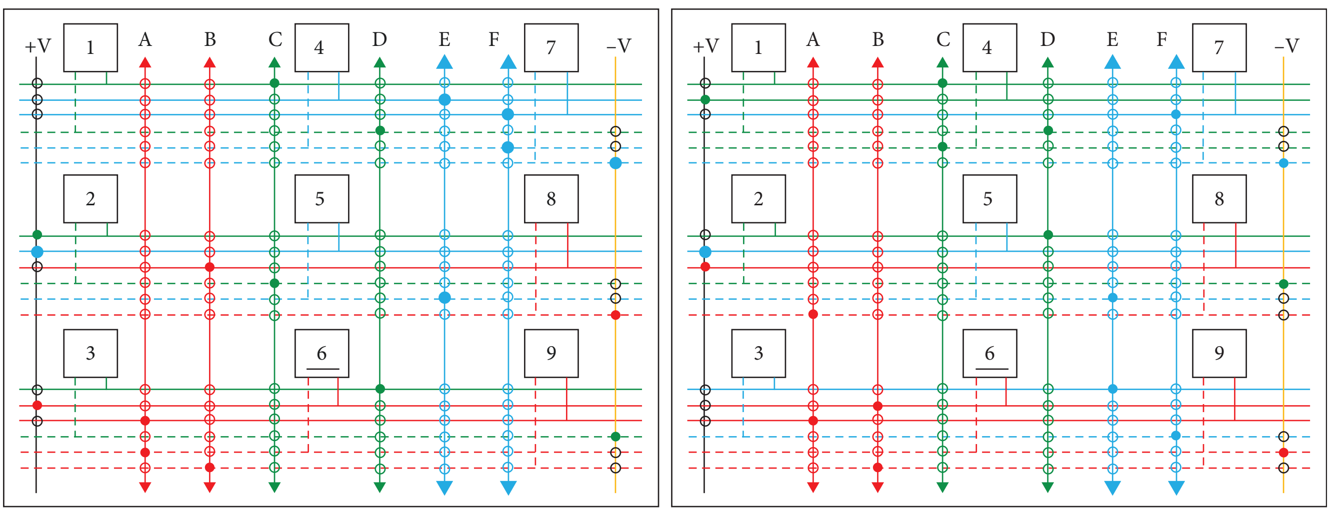

Figure 15: Relay status after reconfiguration for Cases 3 (RT) and 5 (RHT).

appeared after the global peak. Thus, when this system is linked to an optimal power controller, the controller will work at the first local peak. The switching matrix controller works based on an optimization algorithm that takes care of local and global peaks and enhances the power output after reconfiguration.

4.3. DT and Physical World Validation. Generally, DT, i.e., intelligence-provided MATLAB simulation output power and hardware output power are compared and the difference in power, i.e., loss of power due to switching is incorporated into DT as a loss factor during the initial setup trial run by fine-tuning as depicted in Figure 1. In this article, a difference in power output in Tables 3 and 4 is because of unprogrammable load and unregulated ambient circumstances. The goal of achieving increased power output through the use of a reconfiguration controller is accomplished and detailed in the tables. Even though twin and outdoor experimentation results vary to nearly some range, the DT helps the user to predict the output, ensure reliability, schedule maintenance, maintain assets, etc., which, in turn, results in enhanced output, increased efficiency, reduced downtime, etc.

5. Conclusion

Thus, DT is created for addressing partial shading a life-threatening reliability issue for solar assets. An optimization-based switching matrix controller is designed and implemented. It electronically reconfigures panel position by dispersing the shades among rows and columns using optimization algorithms like EID. Its supremacy is compared with one-time static reconfiguration techniques like skyscrapers. DT interacts with the physical world by driven data. Results acquired from DT and the physical world by setting up the actual model of the 3×3 solar panels using solar P–V panels with switching matrix controller have proved that the output of the solar panels during partial shading conditions has been increased to a certain extent of about 30%–45% approximately based on shading cases. It proves economically beneficial by ensuring panel life and increased output power. This DT improves the efficiency of the existing energy system that has been set up in various places. DT has made the hardware setup more reliable, and it also increases the life expectancy of the solar panels and promises a better payback period, thus adding profit for investors.

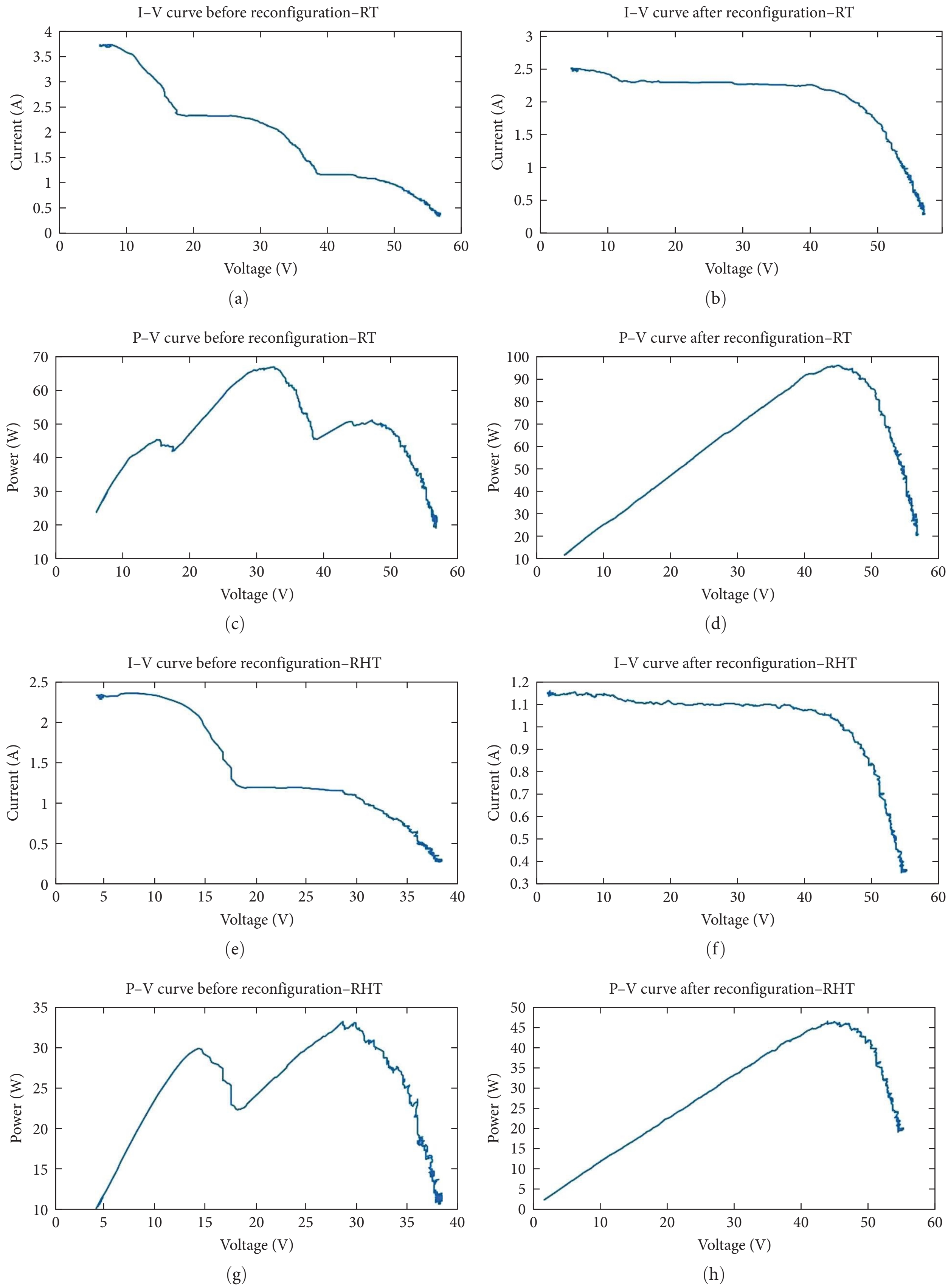

Figure 16: I–V curves and P–V curves of Case 3 (a–d) and Case 5 (e–h).

Table 4: Position vector before and after reconfiguration with power difference.

Case no.	Position before reconfiguration	Position after reconfiguration	Power difference at first peak (W)	Power difference at global peak (W)
	1 4 7	1 4 7	0	0
No shading	2 5 8	2 5 8	—	—
	3 6 9	3 6 9	—	—
1	1 4 7	5 3 9	+50	+30
	2 5 8	2 7 8	—	—
	3 6 9	4 1 6	—	—
2	1 4 7	2 9 5	+5	+5
	2 5 8	4 3 7	—	—
	3 6 9	8 6 1	—	—
3	1 4 7	6 2 5	+50	+30
	2 5 8	9 1 4	—	—
	3 6 9	8 3 7	—	—
4	1 4 7	9 4 5	+23	+15
	2 5 8	8 7 3	—	—
	3 6 9	1 2 6	—	—
5	1 4 7	8 4 5	+17	+13
	2 5 8	9 1 3	—	—
	3 6 9	4 2 7	—	—
6	1 4 7	8 6 1	+7	+7
	2 5 8	5 9 4	—	—
	3 6 9	2 3 7	—	—

Data Availability

This article does not involve data sharing as no data sets were created or analyzed during the current study.

Conflicts of Interest

The authors declare that they have no conflicts of interest.

Acknowledgments

The authors extend their gratitude to the management for their generous support and the comprehensive facilities that facilitated the execution of this research.

References

[1] C. Pylianidis, S. Osinga, and I. N. Athanasiadis, "Introducing digital twins to agriculture," *Computers and Electronics in Agriculture*, vol. 184, Article ID 105942, 2021.

[2] C. Verdouw, B. Tekinerdogan, A. Beulens, and S. Wolfert, "Digital twins in smart farming," *Agricultural Systems*, vol. 189, Article ID 103046, 2021.

[3] B. Brenner and V. Hummel, "Digital twin as enabler for an innovative digital shopfloor management system in the ESB logistics learning factory at Reutlingen University," *Procedia Manufacturing*, vol. 9, pp. 198–205, 2017.

[4] M. Grieves, "Digital twin: manufacturing excellence through virtual factory replication," *White Paper*, vol. 1, pp. 1–7, 2015.

[5] W. Kritzinger, M. Karner, G. Traar, J. Henjes, and W. Sihn, "Digital twin in manufacturing: a categorical literature review and classification," *IFAC-PapersOnLine*, vol. 51, no. 11, pp. 1016–1022, 2018.

[6] B. Björnsson, C. Borrebaeck, N. Elander et al., "Digital twins to personalize medicine," *Genome Medicine*, vol. 12, Article ID 4, 2020.

[7] Y. Liu, L. Zhang, Y. Yang et al., "A novel cloud-based framework for the elderly healthcare services using digital twin," *IEEE Access*, vol. 7, pp. 49088–49101, 2019.

[8] P. Winkler, S. Gallego-García, and M. Groten, "Design and simulation of a digital twin mobility concept: an electric aviation system dynamics case study with capacity constraints," *Applied Sciences*, vol. 12, no. 2, Article ID 848, 2022.

[9] M. Kaliske, R. Behnke, and I. Wollny, "Vision on a digital twin of the road–tire–vehicle system for future mobility," *Tire Science and Technology*, vol. 49, no. 1, pp. 2–18, 2021.

[10] S. Kaewunruen, P. Rungskunroch, and J. Welsh, "A digital-twin evaluation of net zero energy building for existing buildings," *Sustainability*, vol. 11, no. 1, Article ID 159, 2019.

[11] T. I. Zohdi, "A digital-twin and machine-learning framework for the design of multiobjective agrophotovoltaic solar farms," *Computational Mechanics*, vol. 68, pp. 357–370, 2021.

[12] S. R. Madeti and S. N. Singh, "Monitoring system for photovoltaic plants: a review," *Renewable and Sustainable Energy Reviews*, vol. 67, pp. 1180–1207, 2017.

[13] R. Dhaouadi, A. Al-Othman, A. A. Aidan, M. Tawalbeh, and R. Zannerni, "A characterization study for the properties of dust particles collected on photovoltaic (PV) panels in Sharjah, United Arab Emirates," *Renewable Energy*, vol. 171, pp. 133–140, 2021.

[14] M. Dhimish, V. Holmes, P. Mather, and M. Sibley, "Novel hot spot mitigation technique to enhance photovoltaic solar panels output power performance," *Solar Energy Materials and Solar Cells*, vol. 179, pp. 72–79, 2018.

[15] A. Triki-Lahiani, A. Bennani-Ben Abdelghani, and I. Slama-Belkhodja, "Fault detection and monitoring systems for photovoltaic installations: a review," *Renewable and Sustainable Energy Reviews*, vol. 82, Part 3, pp. 2680–2692, 2018.

[16] S. Malathy and R. Ramaprabha, "Reconfiguration strategies to extract maximum power from photovoltaic array under partially shaded conditions," *Renewable and Sustainable Energy Reviews*, vol. 81, Part 2, pp. 2922–2934, 2018.

[17] B. Long-Dong, Y.-K. Wu, and M.-H. Pham, "Fault identification and diagnosis methods for the photovoltaic system: a review," in *2021 7th International Conference on Applied System Innovation (ICASI)*, pp. 126–129, IEEE, Chiayi, Taiwan, September 2021.

[18] C. Buerhop, S. Wirsching, A. Bemm et al., "Evolution of cell cracks in PV-modules under field and laboratory conditions," *Progress in Photovoltaics: Research and Applications*, vol. 26, no. 4, pp. 261–272, 2018.

[19] X. Liu and Y. Wang, "Reconfiguration method to extract more power from partially shaded photovoltaic arrays with series–parallel topology," *Energies*, vol. 12, no. 8, Article ID 1439, 2019.

[20] A. Woyte, J. Nijs, and R. Belmans, "Partial shadowing of photovoltaic arrays with different system configurations: literature review and field test results," *Solar Energy*, vol. 74, no. 3, pp. 217–233, 2003.

[21] S. Pareek, N. Chaturvedi, and R. Dahiya, "Optimal interconnections to address partial shading losses in solar photovoltaic arrays," *Solar Energy*, vol. 155, pp. 537–551, 2017.

[22] P. Romano, R. Candela, M. Cardinale, V. Li Vigni, D. Musso, and E. Riva Sanseverino, "Optimization of photovoltaic energy production through an efficient switching matrix," *Journal of Sustainable Development of Energy, Water and Environment Systems*, vol. 1, no. 3, pp. 227–236, 2013.

[23] R. K. Pachauri, "Imperative role of optimization techniques to reconfigure solar photovoltaic array systems to diminish shading effects," *International Journal of Circuit Theory and Applications*, vol. 50, no. 1, pp. 317–353, 2022.

[24] H. A. Kazem, "Evaluation of PV output in terms of environmental impact based on mathematical and artificial neural network models," *International Journal of Energy Research*, vol. 45, no. 1, pp. 396–412, 2021.

[25] M. S. S. Nihanth, J. P. Ram, D. S. Pillai, A. M. Y. M. Ghias, A. Garg, and N. Rajasekar, "Enhanced power production in PV arrays using a new skyscraper puzzle based one-time reconfiguration procedure under partial shade conditions (PSCs)," *Solar Energy*, vol. 194, pp. 209–224, 2019.

[26] B. I. Rani, G. S. Ilango, and C. Nagamani, "Enhanced power generation from PV array under partial shading conditions by shade dispersion using Su Do Ku configuration," *IEEE Transactions on Sustainable Energy*, vol. 4, no. 3, pp. 594–601, 2013.

[27] A. S. Yadav, R. K. Pachauri, Y. K. Chauhan, S. Choudhury, and R. Singh, "Performance enhancement of partially shaded PV array using novel shade dispersion effect on magic-square puzzle configuration," *Solar Energy*, vol. 144, pp. 780–797, 2017.

[28] B. Dhanalakshmi and N. Rajasekar, "Dominance square based array reconfiguration scheme for power loss reduction in solar PhotoVoltaic (PV) systems," *Energy Conversion and Management*, vol. 156, pp. 84–102, 2018.

[29] K. Bavithra, S. C. Raja, and P. Venkatesh, "Optimal setting of FACTS devices using particle swarm optimization for ATC enhancement in deregulated power system," *IFAC-PapersOnLine*, vol. 49, no. 1, pp. 450–455, 2016.

[30] J. Prasanth Ram and N. Rajasekar, "A new robust, mutated and fast tracking LPSO method for solar PV maximum power point tracking under partial shaded conditions," *Applied Energy*, vol. 201, pp. 45–59, 2017.

[31] S. N. Deshkar, S. B. Dhale, J. S. Mukherjee, T. S. Babu, and N. Rajasekar, "Solar PV array reconfiguration under partial shading conditions for maximum power extraction using genetic algorithm," *Renewable and Sustainable Energy Reviews*, vol. 43, pp. 102–110, 2015.

[32] A. Kumar, M. Rizwan, U. Nangia, and M. Alaraj, "Grey wolf optimizer-based array reconfiguration to enhance power production from solar photovoltaic plants under different scenarios," *Sustainability*, vol. 13, no. 24, Article ID 13627, 2021.

[33] R. V. Mahto, D. K. Sharma, D. X. Xavier, and R. Raghavan, "Improving performance of photovoltaic panel by reconfigurability in partial shading condition," *Journal of Photonics for Energy*, vol. 10, no. 4, Article ID 042004, 2020.

[34] M. Kaffash, K. Bruninx, and G. Deconinck, "Data-driven forecasting of local PV generation for stochastic PV-battery system management," *International Journal of Energy Research*, vol. 45, no. 11, pp. 15962–15979, 2021.